Temperature-dependent band structure evolution determined by surface geometry in organic halide perovskite single crystals

Jinpeng Yang,[1,2,*] Matthias Meissner,[2] Takuma Yamaguchi,[2] Bin Xi,[1] Keishi Takahashi,[3] Shed A. Abd. Rahman,[3] Xianjie Liu ![ORCID],[4] Hiroyuki Yoshida,[3] Mats Fahlman ![ORCID],[4] and Satoshi Kera[2,*]

[1]*College of Physical Science and Technology, Yangzhou University, Jiangsu 225009, China*

[2]*Institute for Molecular Science, Department of Photo-Molecular Science, Myodaiji, Okazaki 444-8585, Japan*

[3]*Graduate School of Engineering, Chiba University, Chiba 263-8522, Japan*

[4]*Laboratory for Organic Electronics, ITN, Linköping University, Norrköping SE-60174, Sweden*

Organic halide perovskites have attracted much attention due to their potential applications in optoelectronic devices. Since the generally higher flexibility compared to their inorganic counterparts, their structures are prone to be more sensitive toward external effects, where the fundamental understanding of their band structure evolutions is still inconclusive. In this study, different electronic structure evolutions of perovskite single crystals are found via angle-resolved photoelectron spectroscopy: (i) Unchanged top valence band (VB) dispersions under different temperatures can be found in the $CH_3NH_3PbI_3$. (ii) Phase transitions induced the evolution of top VB dispersions, and even a top VB splitting with Rashba effects can be observed in the $CH_3NH_3PbBr_3$. Combined with low-energy electron diffraction, metastable atom electron spectroscopy, and density functional theory calculation, we confirm that different band structure evolutions observed in these two perovskite single crystals originated from the cleaved top surface layers, where the different surface geometries with $CH_3NH_3^+$-I in $CH_3NH_3PbI_3$ and Pb-Br in $CH_3NH_3PbBr_3$ are responsible for finding band dispersion change and appearance of the Rashba-type splitting. Such findings suggest that the top surface layer in organic halide perovskites should be carefully considered to create functional interfaces for developing perovskite devices.

I. INTRODUCTION

Organic-inorganic halide perovskites (ABX_3, where A = organic cation, B = Ge, Sn, or Pb, and X = halide ion) have several advantages that facilitate application in optoelectronics, such as long carrier lifetime, large diffusion length, high light absorption coefficient, low exciton binding energy, and easy fabrication [1–5]. As a result, perovskite solar cells are in further development toward commercialization despite a lack of fundamental understanding of several crucial areas. It has been reported that electronic structure at surfaces of perovskite layers could strongly affect charge transport, device performance, and stabilities [3,6,7]. However, the physical understanding of electronic structure in surfaces of perovskites is inconclusive [8–10]. Structure study has recently reported the coexistence and gradual phase transition in these organic halide perovskites, while the mysterious inconsistency of observed band structure and surface structure is still waiting for urgent clarification [8,10–12]. On the other hand, Niesner *et al.* have found the Rashba-type effect induced top valence band (VB) splitting via angle-resolved photoelectron spectroscopy (ARPES) for $CH_3NH_3PbBr_3$ single crystal under both cubic and tetragonal phases [13]. which was later thought due to the surface polar domains and/or surface defects during sample preparation by Che *et al.* [14]. In order to address these controversies and elucidate their origins, a detailed study of the relations between temperature-induced phase transitions at surface structures and evolutions of their electronic structures is then vital, which unfortunately is still lacking.

In this paper, we use angle-resolved photoelectron spectroscopy (ARPES), low-energy electron diffraction (LEED), and metastable atom electron spectroscopy (MAES) techniques to study the evolution of electronic structures and the change in surface geometry at various temperatures of the organic halide perovskite single crystals. We identify different characters of band dispersions between $CH_3NH_3PbBr_3$ and $CH_3NH_3PbI_3$ (A = $CH_3NH_3^+$, B = Pb, and X = Br or I), even though their LEED results yield similar patterns. In contrast to no change of band structures in $CH_3NH_3PbI_3$ single crystal during the decreasing of temperatures, clear band structure evolutions gradually appearing in the top VB splitting can be found in the $CH_3NH_3PbBr_3$ single crystal. Based on additional experimental evidence from ARPES, LEED, and MAES, it is found that different surface geometries cleaved from organic halide perovskites (A-X plane and B-X plane) dominate these various observations in band structures as well as the origin of top VB splitting due to the Rashba-type effect, which strongly suggests to us the importance of preparing a different top surface layer in organic halide perovskites for developing new functional devices.

II. EXPERIMENTAL DETAILS

Organic halide perovskite single crystals were grown by the following methods proposed by Poglitsch and Weber

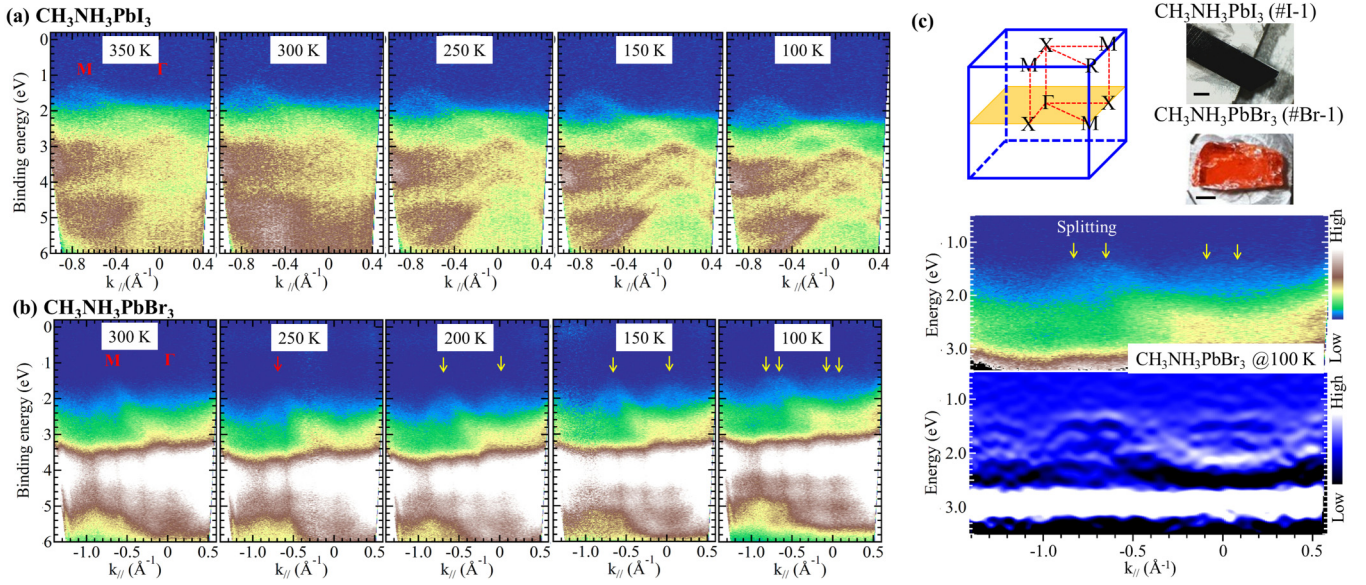---

*Corresponding authors: yangjp@yzu.edu.cn; kera@ims.ac.jp

FIG. 1. Band evolution of the organic halide perovskite single crystals with decreasing temperatures. (a) He I_α-ARPES spectra of the $CH_3NH_3PbI_3$ single crystal (denoted as I-1) along a cubic ΓM ($\Gamma^C M^C$) direction with temperature changes from 350 to 100 K; (b) He I_α-ARPES spectra of the $CH_3NH_3PbBr_3$ (denoted as Br-1) single crystal along the $\Gamma^C M^C$ direction with temperatures changes from 300 to 100 K. (c) Upper part: measured cubic Brillouin zone and cleaved surfaces of $CH_3NH_3PbI_3$ (I-1) and $CH_3NH_3PbBr_3$ (Br-1) crystal samples; bottom part: confirmed Rashba-type splitting (raw data in upper map and second derivative data in lower map) found by ARPES for $CH_3NH_3PbBr_3$ single crystal under 100 K. The black bar in the upper part of (c) is 1 mm.

[15], in which their crystal structures were confirmed using crystal x-ray diffraction (see Supplemental Material Table S1 [16]). All cleaved samples were adhered to molybdenum sample holders by using a silver paste in the atmosphere for a short time ($\sim$2 min), followed by annealing in an ultrahigh vacuum ($<3 \times 10^{-8}$ Pa), while the temperature slowly increased to 350 K (1 h) to confirm surface cleanness. ARPES was performed using a high-sensitivity apparatus with a hemispherical electron energy analyzer (MBS A-1), monochromatic He I_α ($h\nu = 21.22$ eV) radiation source, where the resolution was set to 30 meV. Temperature-dependent LEED measurements were performed in a calibrated microchannel-plate (MCP) LEED device attached to the ARPES UHV chamber. MAES measurements were performed at Chiba University, where metastable He* atoms ($2^3S : 19.82$ eV) were generated by a cold cathode discharging, and He*(2^1S) was eliminated by using a quench lamp (DC helium lamp). The density functional theory (DFT) calculations were performed with Perdew-Burke-Ernzerhof (PBE) generalized gradient approximation (GGA) in Vienna Ab Initio Simulation Package (VASP) [17–20] (see details in the Supplemental Material [16]).

III. RESULTS AND DISCUSSION

Figure 1 depicts the ARPES spectra of (a) $CH_3NH_3PbI_3$ (denoted as I-1) and (b) $CH_3NH_3PbBr_3$ (denoted as Br-1) with decreasing temperatures along the cubic ΓM ($\Gamma^C M^C$) direction. The measured bulk Brillouin zone (BZ) of a cubic phase and two typical samples are also given in the upper part of Fig. 1(c). Our ARPES measurements can only cover the ΓMX plane, which has been confirmed both from our previous result [21] and measured band-gap value

(Fig. S1 [16]). The second-derivative spectra are also provided to enhance visibility, which can be seen in Fig. S2 [16]. As shown in Fig. 1(a), clear band dispersions of the top VB along the $\Gamma^C M^C$ direction for $CH_3NH_3PbI_3$ are obtained under 350 K, in which the top VB near the Γ^C point can be seen with a flat band. In contrast, an apparent change in the top VB at the M^C point is found with a dispersion period of 2×0.70 Å^{-1} and a total energy shift of $\sim$0.7 eV. These observations agree with calculations that only incorporate a cubic phase [8]. Moreover, when measured temperatures become much lower (from 300 to 100 K), the observed dispersion does not demonstrate any change either in the periodicity or in the energy position, which seems to indicate the unchanged surface geometry and related electronic structures. The effective mass can be estimated from these spectra by using the following equation: $m^*(k) = \hbar^2 \times [\partial^2 E(k)/\partial k^2]^{-1}$, where $m^*(k)$, $\hbar$, $E(k)$ and k are the effective mass, reduced Planck's constant, energy, and wave vector, respectively. The $m^* = (0.24 \pm 0.05)m_0$ (m_0 is the free-electron mass) is obtained without any apparent change from temperature reduction.

On the other hand, the ARPES spectra for $CH_3NH_3PbBr_3$ [in Fig. 1(b)] demonstrate remarkable changes in the band dispersions on the top VB compared with results from $CH_3NH_3PbI_3$. At 300 K, we observe a clear band dispersion of the top VB with a maximum at the M^C point ($\sim$0.75 Å^{-1}), consistent with previously reported results [9]. Furthermore, a gradual evolution of the band dispersion on the top VB is seen when the temperature decreases from 300 to 100 K. An additional top VB appears at the Γ point and can be distinguished at both 150 and 100 K, thus indicating that the dispersion period changes from $\sim$2 $\times$ 0.75 Å^{-1} to $\sim$2 $\times$ 0.38 Å^{-1}. More importantly, as shown in Fig. 1(c) with both the raw and
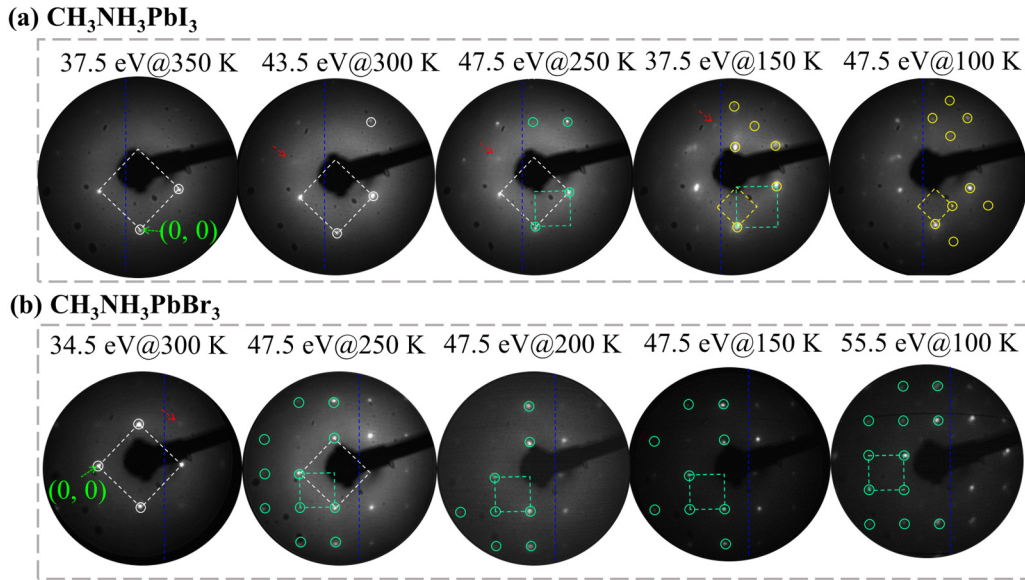
(a) CH₃NH₃PbI₃

(b) CH₃NH₃PbBr₃

FIG. 2. LEED results of the distortion-corrected images of cleaved organic halide perovskites. (a) Surface of the $CH_3NH_3PbI_3$ single crystal (I-1), (b) surface of the $CH_3NH_3PbBr_3$ single crystal (Br-1) measured at various temperatures (as indicated). In $CH_3NH_3PbI_3$, the simulated structures having square unit cells with lattice constants of 6.25 ± 0.02 Å (white), 8.86 ± 0.02 Å (green), and 12.53 ± 0.02 Å (yellow) are superimposed on the right side of each image. In $CH_3NH_3PbBr_3$, the simulated structures with lattice constants of 5.93 ± 0.05 Å (white) and 8.38 ± 0.05 Å (green) are superimposed on the left side of each image.

second derivative spectra of a $CH_3NH_3PbBr_3$ sample measured at 100 K, the top VB at the two Γ points ($k_{//} = 0$ Å^{-1} and ~ 0.75 Å^{-1}) demonstrates a significant splitting-like behavior, confirming the Rashba-type effects proposed by many theorists over the years [14,22–26]. The $m^* = (0.26 \pm 0.05)m_0$ obtained is consistent with a previous report [9] (see detailed fitting in Fig. S3 [16]). Meanwhile, the Rashba parameter, $\alpha_R = 2E_R/k_0$ is estimated to be 3 ± 1 eV Å (with $k_0 = 0.1$ Å^{-1} and $E_R = 0.15$ eV). The influence of surface disorder artificially induced by using N_2 exposure [27] to the band structure evolution has also been revealed for samples (I-2 and Br-2), in which reducing the visibility of the band dispersion can only be found, as shown in Fig. S4 [16]. Additional measurements for different samples to confirm the reproducibility of our results for these two different perovskite materials have also been confirmed, as seen in Fig. S5 (for $CH_3NH_3PbI_3$, I-3) and Fig. S6 (for $CH_3NH_3PbBr_3$, Br-3) [16]. The VB dispersions for $CH_3NH_3PbI_3$ and $CH_3NH_3PbBr_3$ along the $\Gamma^C X^C$ (a cubic phase) direction measured at different temperatures are also shown in Fig. S7 (for I-1 and Br-1) and Fig. S8 (for Br-3). Different band structure evolutions can be also seen between $CH_3NH_3PbI_3$ and $CH_3NH_3PbBr_3$: Fig. S7(a) depicts the unchanged dispersion period and lowest binding energy position of the top VB, while Fig. S8(a) depicts the unchanged dispersion period but changed the lowest binding energy position of the top VB [16].

The different top VB change between $CH_3NH_3PbI_3$ and $CH_3NH_3PbBr_3$ with reducing the temperatures seems to imply the different surface structures, which are initially studied with LEED measurements. As shown in Fig. 2, the distortion-corrected LEED results are provided with measured temperatures changing from 350 to 100 K for $CH_3NH_3PbI_3$ and from 300 to 100 K for $CH_3NH_3PbBr_3$. The simulated

structures with necessary parameters are also superimposed on the half side of each image. In Fig. 2(a), we observe a gradual change in the surface structure with lattice constants of square unit cells varying from 6.25 ± 0.02 Å (white color, both at 350 and 300 K) and 8.86 ± 0.02 Å (green color, at 250 K) to 12.53 ± 0.02 Å (yellow color, both at 150 and 100 K) for the $CH_3NH_3PbI_3$ single crystal, which agrees with the previously reported results with phase changes from cubic, tetragonal, to orthorhombic [15]. The gradual phase transition induces mixed phases that can also be observed in our LEED results marked with red arrows. Weak LEED spots representing a tetragonal phase is found at 300 K and an orthorhombic phase is evident at 150 K. Furthermore, the inconsistency is obviously shown between results from LEED and ARPES since no change of band dispersion in the periodicity is found from ARPES [Fig. 1(a)]. In Fig. 2(b), the surface structure for the $CH_3NH_3PbBr_3$ gives only two different lattice constants of square unit cells among different temperatures, in which one is 5.93 ± 0.05 Å (white color, 300 K, representing a cubic phase) and the other one is 8.38 ± 0.05 Å (green color, from 250 to 100 K, representing a tetragonal phase). Weaker spots representing a tetragonal phase at 300 K can be also found (marked with a red arrow). Different from the inconsistent tendency in $CH_3NH_3PbI_3$, a good agreement can be found in $CH_3NH_3PbBr_3$. The periodic change in LEED results is consistent with ARPES results, where the surface structure changes from a cubic phase to a tetragonal phase.

Moreover, the surface structure has also been further studied by using MAES. Since MAES uses metastable atoms which cannot penetrate the bulk of the solid, it can enable the observation of the outermost surface electrons selectively [28]. The schematic diagram showing the working mechanism of MAES through Penning ionization [28–30] and different
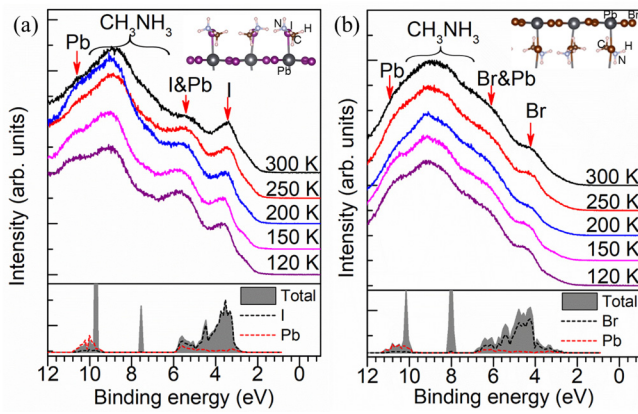
FIG. 3. Temperature-dependent MAES spectra obtained with temperature change from 300 to 120 K for (a) $CH_3NH_3PbI_3$ (I-1) and (b) $CH_3NH_3PbBr_3$ (Br-1) single crystals. Bottom spectra with gray color depict DFT calculated results for valence band with a tetragonal phase, where spectral features are assigned with different elements using dashed lines. Calculated spectra are shifted to fit the experimental data so that spectral features can be assigned with each component independently. The inset shows different top surface atomic structures for a tetragonal phase.

views of perovskite topmost surfaces are given in Figs. S9(a) and S9(b) [16]. Experimental results of MAES for crystal surfaces are shown in Fig. 3. The spectral features are assigned according to the DFT calculation, where the calculated spectra depending on the element for tetragonal phases are shown on the bottom of Fig. 3. In Fig. 3(a), the MAES features keep almost unchanged for an intense top band which is described by the I(5 p) orbital upon the cooling, while it increases for the weak-Pb(6 p)-related bands which are enhanced at the lower temperatures by displacing the surface I atoms. In Fig. 3(b), the MAES features show no clear difference on the temperature, suggesting the orbital distribution at the outermost surface keeps unchanged even if the lateral displacement has occurred upon the cooling. Combing with the different behavior on top surface geometry change in perovskites [shown in Fig. S9(b)] [16], these MAES results indicate that the crystal surface should be composed by different geometries/elements, where the plane A-X ($CH_3NH_3^+$-I) should be for $CH_3NH_3PbI_3$ while the plane B-X (Pb-Br) should be for $CH_3NH_3PbBr_3$. The influences of different phases (cubic or tetragonal) to the spectra shape and the energy positions for each component are negligible [31], yet the arrangements of the orbital spread and/or orientation are rather important to discuss the MAES features. Indeed the relative intensity of halogen-derived bands at around 3.5 eV for $CH_3NH_3PbI_3$ is much stronger than that of $CH_3NH_3PbBr_3$, where the Br orbital is less interactive to the He* due to the large Pb orbital distribution located in the same surface plane. Moreover, the existence of different surfaces with either the plane of A-X or B-X in $CH_3NH_3PbBr_3$ has been reported by Hsu *et al.* with STM measurement [32]. The recent ARPES experiment for another cleaved $CH_3NH_3PbBr_3$ (Br-4) supports the existence of the A-X plane ($CH_3NH_3^+$-Br) with giving no change of the band dispersion under lower temperatures (see Fig. S10 [16]).

The uneasy finding of the B-X plane for $CH_3NH_3PbI_3$ single crystal may be due to different thermodynamical stability, where a $CH_3NH_3^+$-I terminated surface is more stable than a Pb-I terminated surface [33].

Finally, based on our experimental observations combined with the theoretical calculations, the origin of the different evolution in ARPES spectra between $CH_3NH_3PbI_3$ and $CH_3NH_3PbBr_3$ can be elucidated. Figure 4 shows real space representations of surface geometries and the top VB wave functions of (a) a cubic $CH_3NH_3PbI_3$ and (b) a tetragonal $CH_3NH_3PbBr_3$, which depicts the assembly of the wave functions at atoms in different planes. Calculated band structure of $CH_3NH_3PbI_3$ and $CH_3NH_3PbBr_3$ with spin-orbital coupling are also given in Fig. S11 [16]. As shown in Fig. 4, the top VB wave functions are only assembled at the X (X = I or Br) atoms in the $CH_3NH_3^+$-X plane; either forms a cubic phase or a tetragonal phase, suggesting the negligible influence of organic cation contributes to the density of states (DOS) of the top VB. This could be further confirmed between two phases for the same compound materials (i.e., $CH_3NH_3PbBr_3$ in Fig. S12 [16]). Moreover, combined with (i) the direct information on the atomic orbital spread at the outmost surface of single crystals given by MAES, and (ii) the phase transition from cubic to tetragonal mainly changes the arrangement of organic cations in the $CH_3NH_3^+$-X plane (on the left of Fig. 4), it is then reasonable to expect that the unchanged band dispersions in the $CH_3NH_3PbI_3$ single crystal [Fig. 1(a)] are ascribed to the surface geometry with the $CH_3NH_3^+$-I plane. Despite the fact that temperature changes induced different phases (as confirmed from our LEED patterns in Fig. 2) in the $CH_3NH_3PbI_3$ single crystal, the change in the geometry on the $CH_3NH_3^+$-I plane is mainly focused on directions of the organic cations, such that the organic cations do not contribute any wave functions (or DOS) to the top VB, which results in the inconsistency between the ARPES results and LEED results. On the other hand, the consistent experimental results of ARPES and LEED within a different surface geometry of the Pb-Br plane for the $CH_3NH_3PbBr_3$ single crystal should be achieved due to the broad distributions of the top VB wave functions (or DOS) in all surface atoms. Calculated spectrum with considering the Pb-Br terminated top surface also agrees well with our ARPES results [see Fig. 1(c)], where a deeper VB ($\sim$0.4 eV lower than top VB) can be only found for the Pb-Br terminated surface in $CH_3NH_3PbBr_3$ single crystal [34]. The Pb-Br surface plane is also a key to realize the "experimentally visible" Rashba splitting via ARPES, which is also consistent with the prediction from calculations [26]. Consequently, the origin is revealed from the ARPES results to confirm the existence of such a large Rashba-type splitting in organic halide perovskites.

In principle, the DOS distributions measured by ARPES from these materials should not only include the topmost layer since the inelastic mean free path by using He I$_\alpha$ (21.22 eV) should reach a few nanometers from the "universal curve" [35]. However, the "covered" electronic structure from the underlayer could be realized due to the following reasons: (i) The influence of spectral weight transfer, as pointed out by Puppin *et al.* [10], where they proposed periodic potential and perturbing potential from topmost distortion, could easily reduce the orbital intensity and induce the orthorhombic
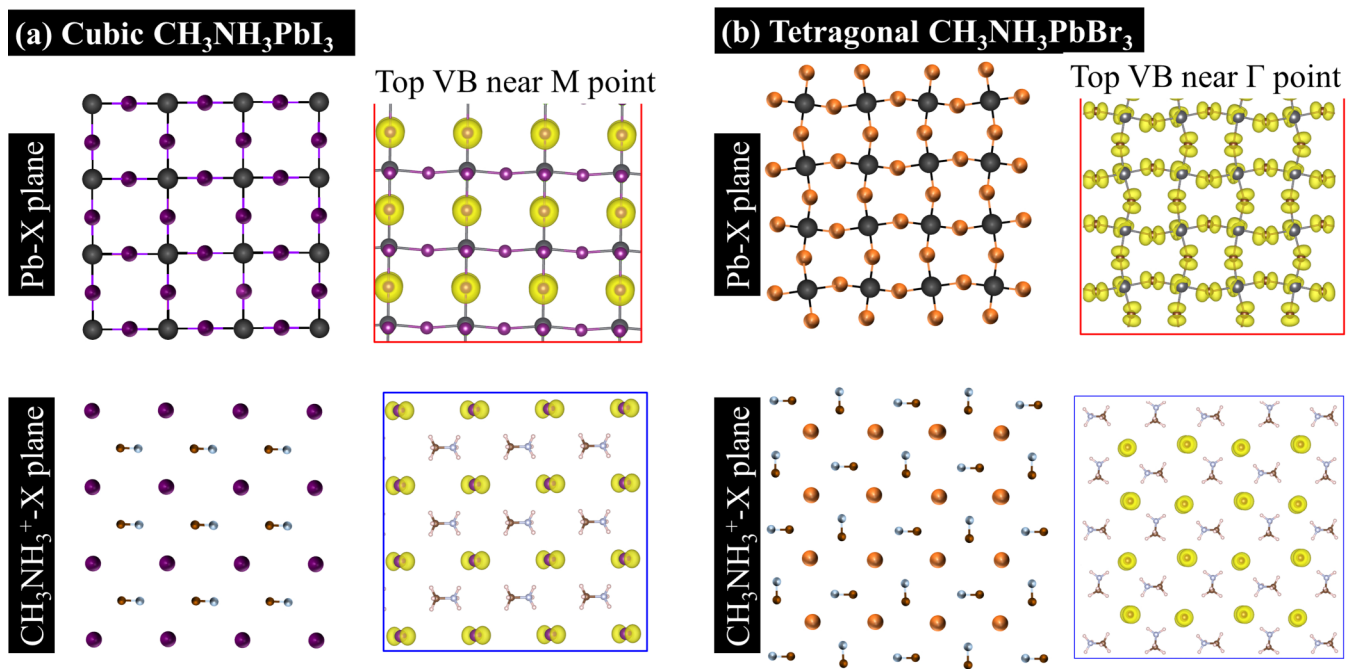
FIG. 4. A real space representation of the top VB wave functions of (a) a cubic $CH_3NH_3PbI_3$ single crystal near M point, and (b) a tetragonal $CH_3NH_3PbBr_3$ single crystal near Γ point, which depicts the assembly of the wave functions at atoms in two different planes (A-X plane and B-X plane, respectively). The left side of each figure shows the atomic arrangements in each plane.

phase to demonstrate a cubic band dispersion. (ii) The low photoionization cross section of Pb-6 s [21], which contributes to the top valence band in organic halide perovskites (Pb-6 s, I-5 p, and Br-4 p), would also make the ARPES "lose" DOS distribution due to photoelectron attenuation if Pb atoms are covered by a $CH_3NH_3^+$-X plane. (iii) The calculations by Angelis have reported that the Pb-X terminated surface with a tetragonal phase should be more favorable in finding the larger Rashba-type splitting [26], which agrees well with our experimental results. From these three additional points, we believe the observed spectra represent electronic structures of the first surface layer with the Rashba splitting in $CH_3NH_3PbBr_3$ single crystal.

IV. SUMMARY

To summarize, we have successfully obtained the temperature-induced evolutions of the electronic structure in organic halide perovskite single crystals, where different characters of band dispersions between $CH_3NH_3PbBr_3$ and $CH_3NH_3PbI_3$ can be found, even though their LEED results yield similar patterns. Combined with MAES results and the DFT computations, these different observations can be well explained after considering the properties of the electronic structures at different crystal surfaces terminations (A-X

plane and B-X plane). The Pb-Br plane on the surface of $CH_3NH_3PbBr_3$ dominates the observations of phase transitions from ARPES as well as the existence of Rashba-type splitting of the top VB. In a tetragonal $CH_3NH_3PbBr_3$, we find that the Rashba-type splitting of the top VB in the momentum space is given by $k_0 = 0.1 \text{ Å}^{-1}$ and $E_R = 0.15$ eV. Such findings are likely to be central for providing direct experimental proof of the novel electronic structure evolutions in organic halide perovskite materials.

All data are available in the main text or the Supplemental Material [16].

[1] A. Kojima, K. Teshima, Y. Shirai, and T. Miyasaka, J. Am. Chem. Soc. **131**, 6050 (2009).

[2] M. Liu, M. B. Johnston, and H. J. Snaith, Nature (London) **501**, 395 (2013).

[3] R. Wang, J. Xue, K. Wang, Z. Wang, Y. Luo, D. Fenning, G. Xu, S. Nuryyeva, T. Huang, Y. Zhao, J. Yang, J. Zhu, M. Wang, S. Tan, I. Yavuz, K. Houk, and Y. Yang, Science **366**, 1509 (2019).

[4] T. M. Brenner, D. A. Egger, L. Kronik, G. Hodes, and D. Cahen, Nat. Rev. Mater. **1**, 15007 (2016).

[5] Y. Fu, H. Zhu, J. Chen, M. P. Hautzinger, X. Y. Zhu, and S. Jin, Nat. Rev. Mater. **4**, 169 (2019).

[6] J. Yin, P. Maity, L. Xu, A. M. El-Zohry, H. Li, O. M. Bakr, J.-L. Bredas, and O. F. Mohammed, Chem. Mater. **30**, 8538 (2018).

[7] Z. Ni, C. Bao, Y. Liu, Q. Jiang, W. Wu, S. Chen, X. Dai, B. Chen, B. Hartweg, Z. Yu, Z. Holman, and J. Huang, Science **367**, 1352 (2020).

[8] J.-P. Yang, M. Meissner, T. Yamaguchi, X.-Y. Zhang, T. Ueba, L.-W. Cheng, S. Ideta, K. Tanaka, X.-H. Zeng, N. Ueno, and S. Kera, Solar RRL **2**, 1800132 (2018).

[9] F. Zu, P. Amsalem, D. A. Egger, R. Wang, C. M. Wolff, H. Fang, M. A. Loi, D. Neher, L. Kronik, S. Duhm, and N. Koch, J. Phys. Chem. Lett. **10**, 601 (2019).

[10] M. Puppin, S. Polishchuk, N. Colonna, A. Crepaldi, D. N. Dirin, O. Nazarenko, R. De Gennaro, G. Gatti, S. Roth, T. Barillot, L. Poletto, R. P. Xian, L. Rettig, M. Wolf, R. Ernstorfer, M. V. Kovalenko, N. Marzari, M. Grioni, and M. Chergui, Phys. Rev. Lett. **124**, 206402 (2020).

[11] L. T. Schelhas, J. A. Christians, J. J. Berry, M. F. Toney, C. J. Tassone, J. M. Luther, and K. H. Stone, ACS Energy Lett. **1**, 1007 (2016).

[12] T. W. Kim, S. Uchida, T. Matsushita, L. Cojocaru, R. Jono, K. Kimura, D. Matsubara, M. Shirai, K. Ito, H. Matsumoto, T. Kondo, and H. Segawa, Adv. Mater. **30**, 1705230 (2018).

[13] D. Niesner, M. Wilhelm, I. Levchuk, A. Osvet, S. Shrestha, M. Batentschuk, C. Brabec, and T. Fauster, Phys. Rev. Lett. **117**, 126401 (2016).

[14] X. Che, B. Traore, C. Katan, M. Kepenekian, and J. Even, Phys. Chem. Chem. Phys. **20**, 9638 (2018).

[15] A. Poglitsch and D. Weber, J. Chem. Phys. **87**, 6373 (1987).

[16] See Supplemental Material at http://link.aps.org/supplemental/10.1103/PhysRevB.102.245101 for additional details about band structure calculation, experimental crystal structure measurements, UPS-LEIPS spectrum, ARPES spectrum (including N_2-exposure effects, different samples, and different k space), and MAES spectrum elucidation.

[17] G. Kresse and J. Furthmuller, Comput. Mater. Sci. **6**, 15 (1996).

[18] G. Kresse and J. Furthmuller, Phys. Rev. B **54**, 11169 (1996).

[19] J. P. Perdew, K. Burke, and M. Ernzerhof, Phys. Rev. Lett. **77**, 3865 (1996).

[20] J. Heyd, G. E. Scuseria, and M. Ernzerhof, J. Chem. Phys. **118**, 8207 (2003).

[21] J. Yang, S. Ren, T. Yamaguchi, M. Meissner, L. Cheng, L. Zhou, S. Ideta, K. Tanaka, and S. Kera, Appl. Phys. Express **13**, 011009 (2020).

[22] F. Zheng, L. Z. Tan, S. Liu, and A. M. Rappe, Nano Lett. **15**, 7794 (2015).

[23] T. Etienne, E. Mosconi, and F. D. Angelis, J. Phys. Chem. Lett. **7**, 1638 (2016).

[24] S. McKechnie, J. M. Frost, D. Pashov, P. Azarhoosh, A. Walsh, and M. van Schilfgaarde, Phys. Rev. B **98**, 085108 (2018).

[25] M. Kim, J. Im, A. J. Freeman, J. Ihm, and H. Jin, Proc. Natl. Acad. Sci. USA **111**, 6900 (2014).

[26] E. Mosconi, T. Etienne, and F. D. Angelis, J. Phys. Chem. Lett. **8**, 2247 (2017).

[27] C. Wang, B. R. Ecker, H. Wei, J. Huang, and Y. Gao, J. Phys. Chem. C **122**, 3513 (2018).

[28] Y. Harada, S. Masuda, and H. Ozaki, Chem. Rev. **97**, 1897 (1997).

[29] S. Kera, H. Yamane, H. Honda, H. Fukagawa, K. K. Okudaira, and N. Ueno, Surf. Sci. **566**, 571 (2004).

[30] S. Kera, Y. Yabuuchi, H. Yamane, H. Setoyama, K. K. Okudaira, A. Kahn, and N. Ueno, Phys. Rev. B **70**, 085304 (2004).

[31] L. Zhou, A. J. Neukirch, D. J. Vogel, D. S. Kilin, L. Pedesseau, M. A. Carignano, A. D. Mohite, J. Even, C. Katan, and S. Tretiak, ACS Energy Lett. **3**, 787 (2018).

[32] H.-C. Hsu, B.-C. Huang, S.-C. Chin, C.-R. Hsing, D.-L. Nguyen, M. Schnedler, R. Sankar, R. E. D.-Borkowski, C.-M. Wei, C.-W. Chen, P. Ebert, and Y.-P. Chiu, ACS Nano **13**, 4402 (2019).

[33] W. Geng, C.-J. Tong, Z.-K. Tang, C. Y. Yam, Y.-N. Zhang, W.-M. Lau, and L.-M. Liu, J. Materiomics **1**, 213 (2015).

[34] T. Komesu, X. Huang, T. R. Paudel, Y. B. Losovyj, X. Zhang, E. F. Schwier, Y. Kojima, M. Zheng, H. Iwasawa, K. Shimada, M. I. Saidaminov, D. Shi, A. L. Abdelhady, O. M. Bakr, S. Dong, E. Y. Tsymbal, and P. A. Dowben, J. Phys. Chem. C **120**, 21710 (2016).

[35] S. Béchu, M. Ralaiarisoa, A. Etcheberry, and P. Schulz, Adv. Energy Mater. **10**, 1904007 (2020).

Correction: The formatting of the sixth author's name contained an error and has been fixed.